

Supporting Information

Reversible Transition of Volatile and Nonvolatile Switching in Ag–In–Zn–S Quantum Dot-Based Memristors with Low Power Consumption for Synaptic Applications

Nan He[†], Langyi Tao[†], Qiangqiang Zhang[†], Xiaoyan Liu[†], Xiaojuan Lian[†], Xiang Wan[†], Er-Tao Hu[†], Lin He[†], Yang Sheng^{,‡}, Feng Xu^{*,†}, and Yi Tong^{*,†}*

[†]College of Electronic and Optical Engineering and College of Microelectronics, Nanjing University of Posts and Telecommunications, 9 Wenyuan Road, Nanjing, Jiangsu 210023, China

[‡]Jiangsu Key Laboratory of Environmentally Friendly Polymeric Materials, School of Materials Science and Engineering, Changzhou University, Changzhou 213164, China

*Email: shengyang@cczu.edu.cn; feng.xu@njupt.edu.cn; tongyi@njupt.edu.cn

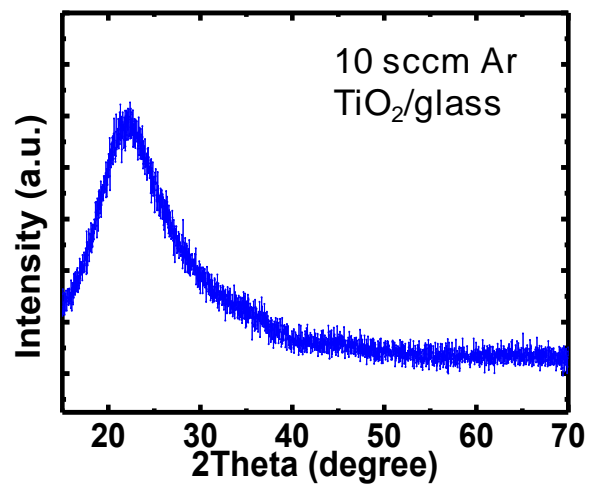


Figure S1. XRD image of TiO₂ grown on glass substrate.

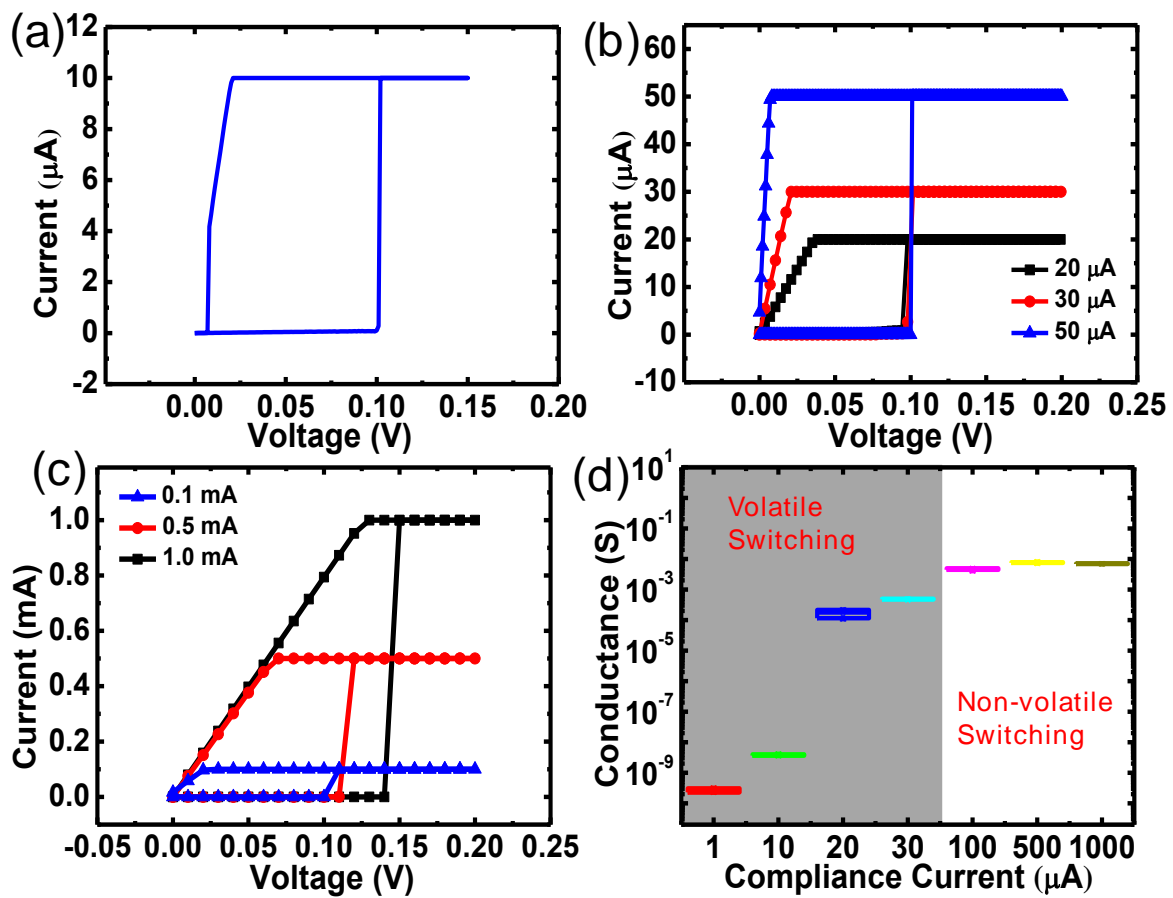


Figure S2. The RS characteristics of QD-based device under the compliance current of a) $10\ \mu$ A, (b) 20 , 30 , and $50\ \mu$ A, (c) 0.1 , 0.5 , and $1.0\ mA$. (d) The relationship between the high conductance state and the compliance current.

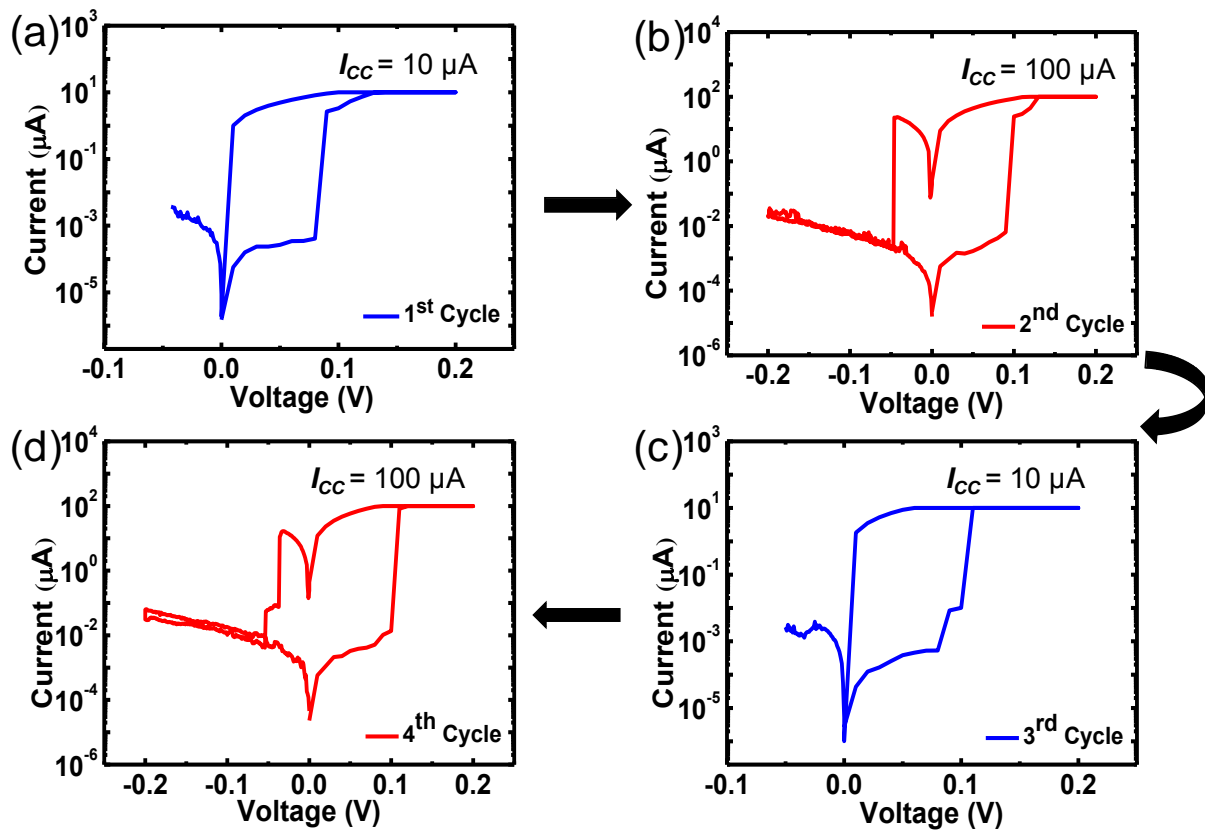


Figure S3. The reversible transitions between the volatile and nonvolatile RS behaviors can be tuned in a single QD-based device.

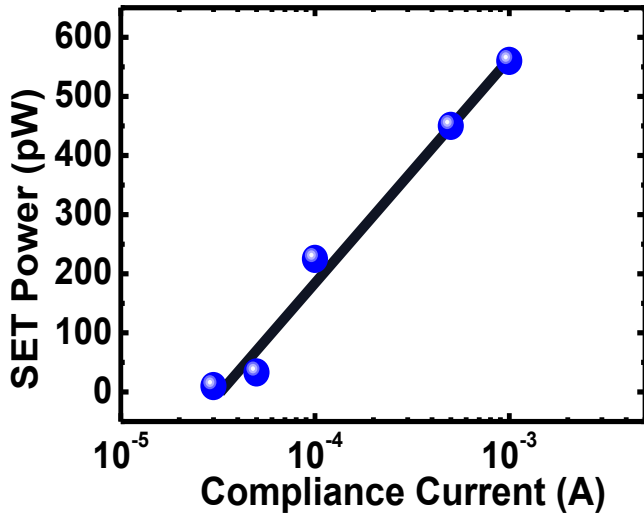


Figure S4. Relationship between the SET power and compliance current for QD-based device.

The SET power (P_{SET}) is calculated by the following equation: $P_{\text{SET}} = V_{\text{SET}} \times I_{\text{SET}}$. I_{SET} is the current of V_{SET} . The P_{SET} of QD-based device under I_{CC} of $30 \mu\text{A}$ has been calculated $\sim 10 \text{ pW}$, as shown in the label of Figure 2a, which shows a relatively ultralow power consumption. Table S1 and S2 respectively show the comparisons of P_{SET} with other TS or Ag-based memristors.

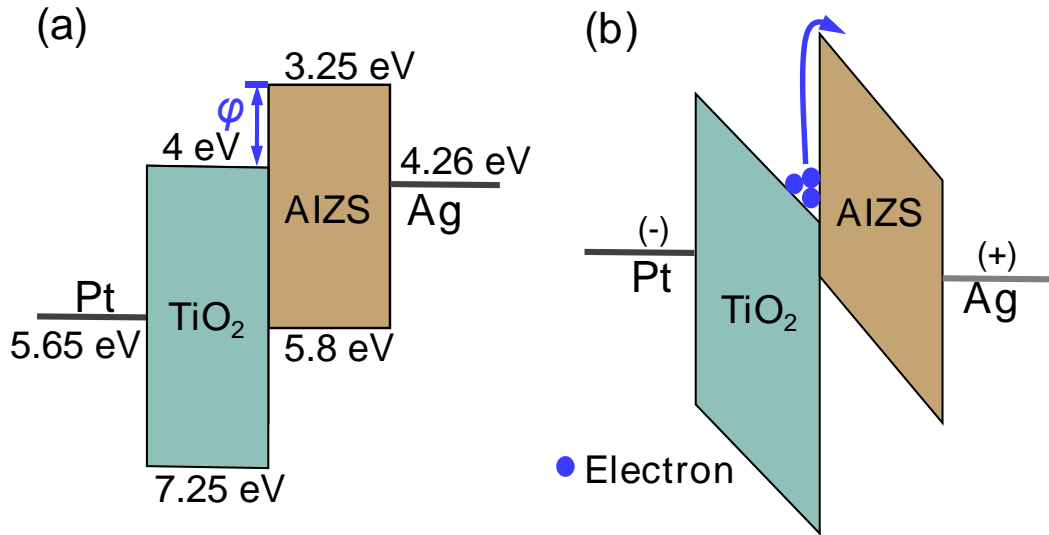


Figure S5. Schematic illustration of energy band diagram of the QD-based device. a) Virgin device (unbiased). (b) Under the SET process.

As shown schematically in Figure S5a, the work function of Pt and Ag are 5.65 eV and 4.26 eV, respectively.¹ The electronic affinity of the amorphous TiO₂ is 4.0 eV and the broad bandgap of TiO₂ and AIZS are approximately 3.25 and 2.55 eV respectively, as reported in the literature.^{2,3} From the above descriptions, we can obviously find out that the potential barrier between TiO₂ and AIZS is 0.75 eV. We can conclude that the insertion of AIZS QDs increases the energy barrier (Figure S5b), which might be the reason why Schottky emission can explain the conduction mechanism of HRS.

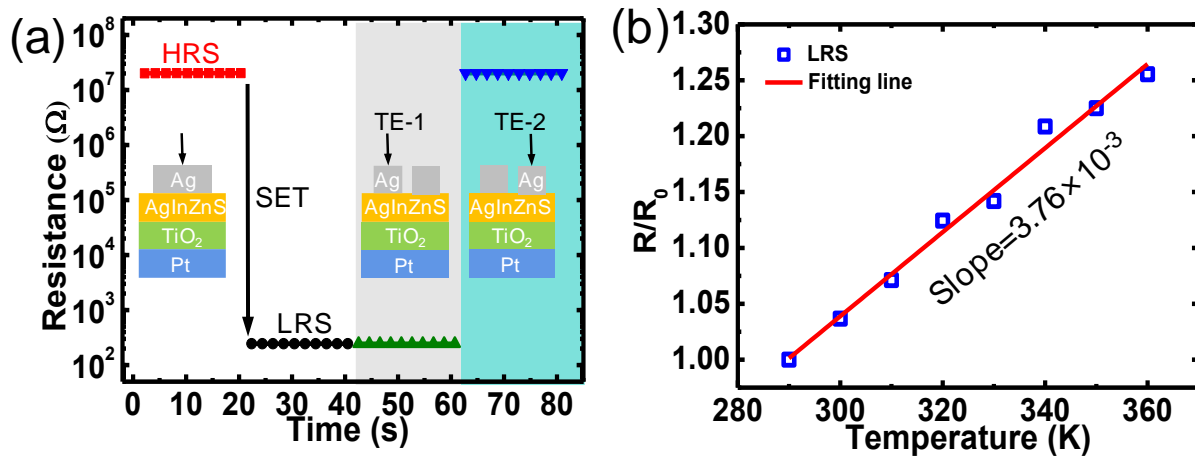


Figure S6. (a) The Ag top electrode was cut into two parts and the resistance values of each part were measured to validate the local behavior of CFs. (b) Relationship between LRS and temperature for illustrating the properties of CFs.

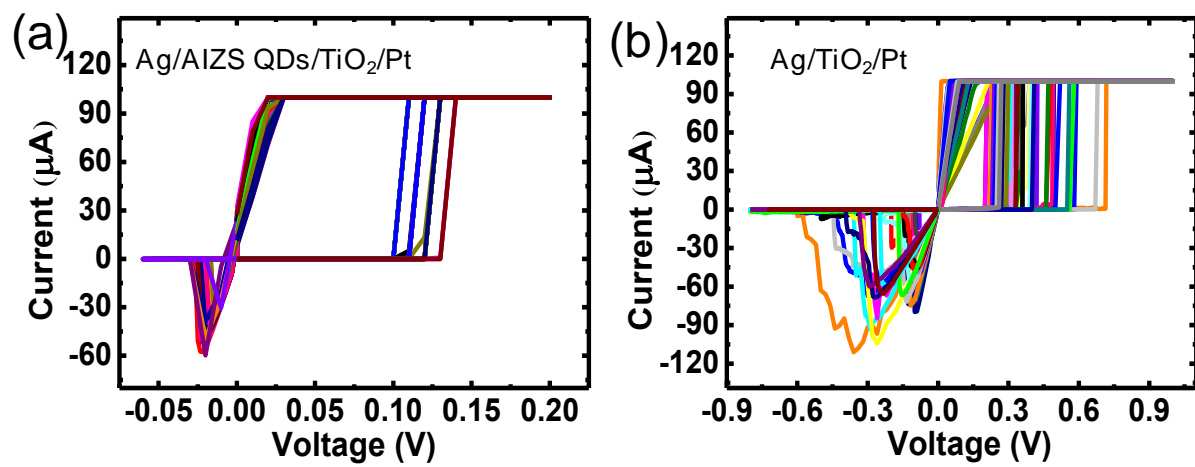


Figure S7. The I - V curves of (a) the Ag/AIZS QDs/TiO₂/Pt device and (b) Ag/TiO₂/Pt device.

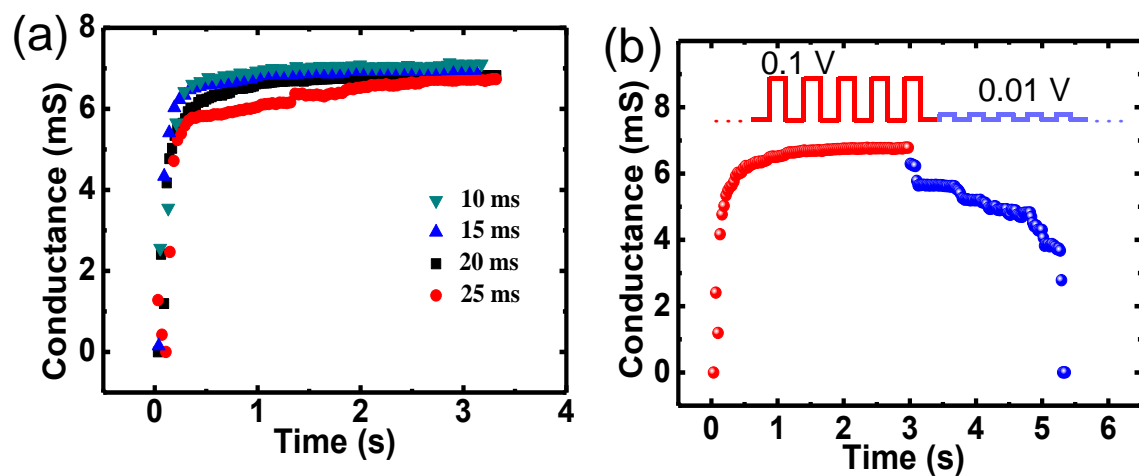


Figure S8. (a) Impact of time interval of the positive pulse trains on conductance modulation. (b) The process of automatic conductivity reduction was recorded with a low read voltage (0.01 V) after the QD-based device conductance was saturated.

Table S1. Comparison of device parameters with memristors with TS characteristics.

Device Structure	SET Voltage [V]	Switching Ratio	I_{cc} [μA]	SET Power [W]	Ref.
Ag/Ag-In-Zn-S/TiO ₂ /Pt	0.08	$\sim 10^5$	30	$\sim 10^{-11}$	This work
Ag/ZrO ₂ /Pt	0.25	$\sim 10^4$	100	$\sim 10^{-9}$	[4]
Pt/ferritin/Pt	0.85	N.A.	5	$\sim 10^{-9}$	[5]
Cu/TaO _x /δ-Cu/Pt	1.3	$\sim 10^2$	50	$\sim 10^{-6}$	[6]
Cu/GeTe/Al ₂ O ₃ /Pt	0.7	N.A.	200	$\sim 10^{-7}$	[7]
TiN/TiO ₂ /NbO _x /Pt	1.3	N.A.	1000	$\sim 10^{-5}$	[8]
Ag/MnO ₂ /Ag	3.0	$\sim 10^4$	10	$\sim 10^{-9}$	[9]
Ag/NiO/Pt	0.8	$\sim 10^2$	1000	$\sim 10^{-5}$	[10]
TiN/VO ₂ /TaO _x /Pt	2.2	N.A.	1000	$\sim 10^{-4}$	[11]
Ag/InP/ZnS/ITO	0.75	N.A.	100	$\sim 10^{-8}$	[12]

Table S2. Comparison of the performance parameters with other devices using Ag electrode.

Device Structure	SET Voltage [V]	RESET Voltage [V]	Retention [s]	Switching Ratio	SET Power	Ref.
Ag/Ag-In-Zn-S/TiO ₂ /Pt	0.08 (TS) 0.15 (MS)	N.A. -0.05	N.A. 10 ⁴	10 ⁵ 10 ⁵	10 pW 0.56 nW	This work
Ag/TiO ₂ : Ag/Pt	0.2	-0.3	N.A.	N.A.	0.6 mW	[13]
Pt-Ag/SiO ₂ : Ag/TiO ₂ /P ⁺⁺ -Si	2.5	-1.5	N.A.	10 ²	5 mW	[14]
Ag/ZnO/Pt	2.1	-0.5	10 ³	10 ¹	2.4 mW	[15]
Ag/TiO ₂ /Pt	0.5	-1.2	N.A.	10 ¹	0.5 mW	[16]
Ag/ZrO ₂ /MoS ₂ /Pt	0.8	-0.25	10 ⁴	10 ⁵	0.5 μW	[17]
Ag/HC(NH ₂) ₂ PbI ₃ /Pt	0.22	-0.6	10 ³	10 ⁵	6.6 nW	[18]
Ag/GaSe/Ag	1.4	-1.1	10 ⁴	10 ⁵	0.9 μW	[19]

Supporting References

- (1) Guan, J. N.; Li, L.; Chen, C. H.; Lu, P.; Yan, Y.; Wang, Z. R.; Lu, N.; Huo, M. X. Enhanced Solar-Photocatalytic Activity for the Simultaneous Degradation and Detoxification of Multiple Chlorophenols by Embedding Plasmonic Pt into $\text{TiO}_2/\text{H}_3\text{PW}_{12}\text{O}_{40}$ nanopore. *Appl. Surf. Sci.* **2020**, *513*, 145833.
- (2) Mora-Fonz, D.; Kaviani, M.; Shluger, AL. Disorder-Induced Electron and Hole Trapping in Amorphous TiO_2 . *Phys. Rev. B*. **2020**, *102*, 054205.
- (3) Choi, D. B.; Kim, S.; Yoon, H. C.; Ko, M.; Yang, H.; Do, Y. R. Color-tunable Ag-In-Zn-S Quantum-Dot Light-Emitting Devices Realizing Green, Yellow and Amber Emissions. *J. Mater. Chem. C* **2017**, *5*, 953–959.
- (4) Du, Gang.; Wang, Chao.; Li, H. X.; Mao, Q. N.; Ji, Z. G. Bidirectional Threshold Switching Characteristics in $\text{Ag/ZrO}_2/\text{Pt}$ Electrochemical Metallization Cells. *AIP Adv.* **2016**, *6*, 085316.
- (5) Zhang, C.; Shang, J.; Xue, W.; Tan, H.; Pan, L.; Yang, X.; Guo, S.; Hao, J.; Liu, G.; Li, R. W. Convertible Resistive Switching Characteristics Between Memory Switching and Threshold Switching in a Single Ferritin-Based Memristor. *Chem. Commun.* **2016**, *52*, 4828–4831.
- (6) Li, H. Y.; Huang, X. D.; Yuan, J. H.; Lu, Y. F.; Wan, T. Q.; Li, Y.; Xue, K. H.; He, Y. H.; Xu, M.; Tong, H.; Miao, X. S. Controlled Memory and Threshold Switching Behaviors in a Heterogeneous Memristor for Neuromorphic Computing. *Adv. Electron. Mater.* **2020**, *6*, 2000309.
- (7) Li, H. Y.; Huang, X. D.; Yuan, J. H.; Lu, Y. F.; Wan, T. Q.; Li, Y.; Xue, K. H.; He, H. Y.; Xu, M.; Tong, H.; Miao, X. S. Controlled Memory and Threshold Switching Behaviors in a Heterogeneous Memristor for Neuromorphic Computing. *Adv. Electron. Mater.* **2020**, *6*, 2000309.

- (8) Luo, Q.; Zhang, X. M.; Yu, Jie.; Wang, W.; Gong, T. C.; Xu, X. X.; Yin, J. H.; Yuan, P.; Tai, L.; Dong, D. N.; Lv, H. B.; Long, S. B; Liu, Q.; Liu, M. Memory Switching and Threshold Switching in a 3D Nanoscaled NbO_x System. *IEEE Electron Device Lett.* **2019**, *40*, 718–721.
- (9) Tu, M. L.; Lu, H. P.; Luo, S. W.; Peng, H.; Li, S. D.; Ke, Y. Z.; Yuan, S. G.; Huang, W.; Jie, W. J.; Hao, J. H. Reversible Transformation Between Bipolar Memory Switching and Bidirectional Threshold Switching in 2D Layered K-birnessite Nanosheets, *ACS Appl. Mater. Interfaces* **2020**, *12*, 24133–24140.
- (10) Li, Y.; Fang, P. W.; Fan, X. H.; Pei, Y. L. NiO-Based Memristor with Three Resistive Switching Modes. *Semicond. Sci. Technol.* **2020**, *35*, 055004.
- (11) Wang, Z. W.; Zheng, Q. L.; Kang, J.; Yu, Z. Z.; Zhong, G. F.; Ling, Y. T.; Bao, L.; Bao, S. Y.; Bai, G. D.; Zheng, S.; Cai, Y. M.; Robertson, J.; Huang, R. Self-Activation Neural Network Based on Self-Selective Memory Device with Rectified Multilevel States. *IEEE Trans. Electron Devices* **2020**, *67*, 4166–4171.
- (12) Wang, J. J.; Lv, Z. Y.; Xing, X. C.; Li, X. G.; Wang, Y.; Chen, M.; Pang, G. J.; Qian, F. S.; Zhou, Y.; Han, S. T. Optically Modulated Threshold Switching in Core-Shell Quantum Dot Based Memristive Device. *Adv. Funct. Mater.* **2020**, *30*, 1909114.
- (13) Yan, X.; Zhao, J.; Liu, S.; Zhou, Z.; Liu, Q.; Chen, J.; Liu, X. Memristor with Ag \square Cluster \square Doped TiO₂ Films as Artificial Synapse for Neuroinspired Computing. *Adv. Funct. Mater.* **2018**, *28*, 1705320.
- (14) Li, D.; Llyas, N.; Li, C.; Jiang, X. D.; Jiang, Y. D.; Li, W. Synaptic Learning and Memory Functions in SiO₂: Ag/TiO₂ Based Memristor Devices. *J. Phys. D: Appl. Phys.* **2020**, *53*, 175102.

- (15) Bejtka, K.; Milano, G.; Ricciardi, C.; Pirri, C. F.; Porro, S. TEM Nanostructural Investigation of Ag-Conductive Filaments in Polycrystalline ZnO-Based Resistive Switching Devices. *ACS Appl. Mater. Interfaces* **2020**, *12*, 29451–29460.
- (16) Lai, C. H.; Chen, C. H.; Tseng, T. Y. Resistive Switching Behavior of Sol-Gel Deposited TiO₂ Thin Films under Different Heating Ambience. *Surf. Coat. Technol.* **2013**, *231*, 399–402.
- (17) Wu, F.; Si, S. Y.; Cao, P.; Wei, W. X.; Zhao, L.; Shi, T.; Zhang, X. M.; Ma, J. W.; Cao, R. R.; Liao, L.; Tseng, T. Y.; Liu, Q. Interface Engineering via MoS₂ Insertion Layer for Improving Resistive Switching of Conductive-Bridging Random Access Memory. *Adv. Electron. Mater.* **2019**, *5*, 1800747.
- (18) J. M. Yang, S. G. Kim, J. Y. Seo, C. Cuhadar, D. Y. Son, D. Lee, and N. G. Park, 1D Hexagonal HC(NH₂)₂PbI₃ for Multilevel Resistive Switching Nonvolatile Memory. *Adv. Electron. Mater.* **2018**, *4*, 1800190.
- (19) Y. Yang, H. Y. Du, Q. Xue, X. H. Wei, Z. B. Yang, C. G. Xu, D. M. Li, W. J. Jie, and J. H. Hao, Three-Terminal Memtransistors Based on Two-Dimensional Layered Gallium Selenide Nanosheets for Potential Low-Power Electronics Applications. *Nano Energy* **2019**, *57*, 566–573.